The International Journal of Advanced Manufacturing Technology (2018) 97:2099–2109
https://doi.org/10.1007/s00170-018-2075-x

ORIGINAL ARTICLE

Material removal mechanism in rotary ultrasonic machining of high-volume fraction SiCp/Al composites

Huiting Zha[1] · Pingfa Feng[1,2,3] · Jianfu Zhang[1,2] · Dingwen Yu[1] · Zhijun Wu[1]

Received: 18 December 2017 / Accepted: 24 April 2018 / Published online: 7 May 2018

Abstract

High-volume fraction silicon carbide-reinforced aluminum matrix (SiCp/Al) composites are widely used in many industrial fields due to their excellent material properties. However, these composites are regarded as one of the most difficult-to-machine materials, owing to the presence of many hard and brittle SiC reinforcements. Rotary ultrasonic machining (RUM) is an effective processing method for SiCp/Al composites. The material removal mechanism in RUM of SiCp/Al composites was investigated by comparing the deformation characteristics of the composites in ultrasonic vibration-assisted scratch (UVAS) tests and conventional scratch (CS) tests which were performed on a rotary ultrasonic machine. The influence of ultrasonic vibration on the machining process was analyzed. Furthermore, the morphologies of the scratching surfaces, scratching forces, and material removal process were evaluated in detail. The theoretical and experimental results revealed that ultrasonic vibration changes the interaction between the cutting tool and the workpiece. The vibration enhanced the Al matrix and facilitated SiC reinforcements removal by increasing the cracks in them. Therefore, the scratching forces in UVAS were smaller and more stable than those in CS. The coefficient of friction (COF) was also smaller than that of CS and hence, the adhesion effect of Al matrix during the scratching process was weakened. This study shows that the removal mode of SiC reinforcements plays a decisive role in the formation of the machined surface. These results can serve as a guide for selecting appropriate processing parameters to obtain improved machining quality of SiCp/Al composites.

Keywords SiCp/Al composites · Rotary ultrasonic machining · Material removal mechanism · Ultrasonic-assisted scratching test

Nomenclature

v_x	Feed velocity in x direction
v_y	Feed velocity in y direction;
v_z	Feed velocity in z direction;
x_0	Initial position in x direction;
y_0	Initial position in y direction;
z_0	Initial position in z direction;
n	Spindle speed;
A	Ultrasonic amplitude;
θ	Penetration angle;
θ_{max}	Maximum penetration angle;
a_z	Acceleration along z direction;
F_y	Tangential force;
F_n	Axial force;
f	Frequency of ultrasonic vibration;
r	Distance from the abrasive grain to the center of the cutting tool;
SiCp/Al	Silicon carbide-reinforced aluminum matrix composites;
RUM	Rotary ultrasonic machining;
UVAS	Ultrasonic vibration-assisted scratch test;
CS	Conventional scratch test;
COF	Coefficient of friction;
CG	Conventional grinding;
SEM	Scanning electron microscope.

✉ Jianfu Zhang
zhjf@tsinghua.edu.cn

[1] Beijing Key Lab of Precision/Ultra-precision Manufacturing Equipments and Control, Department of Mechanical Engineering, Tsinghua University, Beijing 100084, China

[2] State Key Laboratory of Tribology, Department of Mechanical Engineering, Tsinghua University, Beijing 100084, China

[3] Division of Advanced Manufacturing, Graduate School at Shenzhen, Tsinghua University, Shenzhen 518055, China

1 Introduction

High-volume fraction silicon carbide-reinforced aluminum matrix (SiCp/Al) composites have excellent physical and mechanical properties. These include a high specific strength and specific stiffness, relatively high thermal conductivity, low density and thermal expansion coefficient, and good wear resistance [1–3]. SiCp/Al composites are widely used in aerospace, automotive industry, electronics industry, and other fields [4–6]. However, high-volume fraction SiCp/Al composites are considered as one of difficult-to-machine materials owing to the presence of many hard and brittle SiC reinforcements. Although net-shape forming technology is employed in the manufacture of these composites, machining is still essential for meeting their assembly and application requirements. Many problems are encountered in machining high-volume fraction SiCp/Al composites. As the properties of SiC reinforcements completely differ from those of Al matrix, the material deformation process is very complex and achieving good surface integrity is difficult [7, 8]. SiC reinforcements can break and fall off resulting in many defects on the composites. Subsurface damage may also occur during the machining process [9] and edge chippings are easily formed at the edge of the workpieces [10]. Accordingly, ensuring the service life and reliability of products is difficult. Moreover, due to the high hardness of SiC reinforcements, tool wear is severe [11, 12] and common tools made by high-speed steel or carbide are unable to meet the machining demand which will notably increase the manufacturing cost.

Rotary ultrasonic machining (RUM), a hybrid machining process which combines conventional ultrasonic vibrating machining and grinding, has received significant attention recently. As Fig. 1 shows, the ultrasonic vibration is superimposed on the cutting tools in RUM. Hollow diamond grain tools are usually used and the machining process is conducted on a NC machining center. In terms of complex surface machining, RUM has obvious superiority over conventional grinding (CG) [13, 14]. Numerous studies have confirmed that RUM is an effective method for machining hard and brittle materials, such as ceramics, optical materials, and high-volume fraction metal matrix composites [15–17]. Many researchers found that RUM can reduce the cutting force during the machining process and improve the surface quality [18–20]. Conventional machining processes for high-volume fraction SiCp/Al composites have been extensively investigated. Huang et al. [21] observed the machined surface morphologies by conventional grinding method and analyzed the chip formation mechanism. Zhou et al. [22] evaluated the drilling characteristics (drilling forces, tool wear, surface roughness, and entrance edge quality) during the machining of SiCp/Al composites with electroplated diamond drills. However, the material removal mechanism in RUM of SiCp/Al composites has rarely been studied. Revealing the influence of ultrasonic vibration on the machining process can elucidate RUM of SiCp/Al composites and serve as a guide in the selection of appropriate processing parameters.

The scratching test has been used to evaluate the deformation behaviors and tribological properties of materials. These tests can provide primary information about the material removal behavior manifested through the scratching surface morphologies. Furthermore, researchers can observe the interaction between the tool and the material intuitively. Zhang et al. [23] compared the scratching characteristics of sapphire crystal in ultrasonic vibration-assisted scratch (UVAS) tests and conventional scratch (CS) tests. The results showed that there are two different material removal mode in CS tests, i.e., plastic removal and brittle removal, whereas only plastic removal mode existed in UVAS tests. Cao et al. [24] found there were three material removal modes (plastic removal, brittle-plastic transition, and brittle removal) in scratching SiC

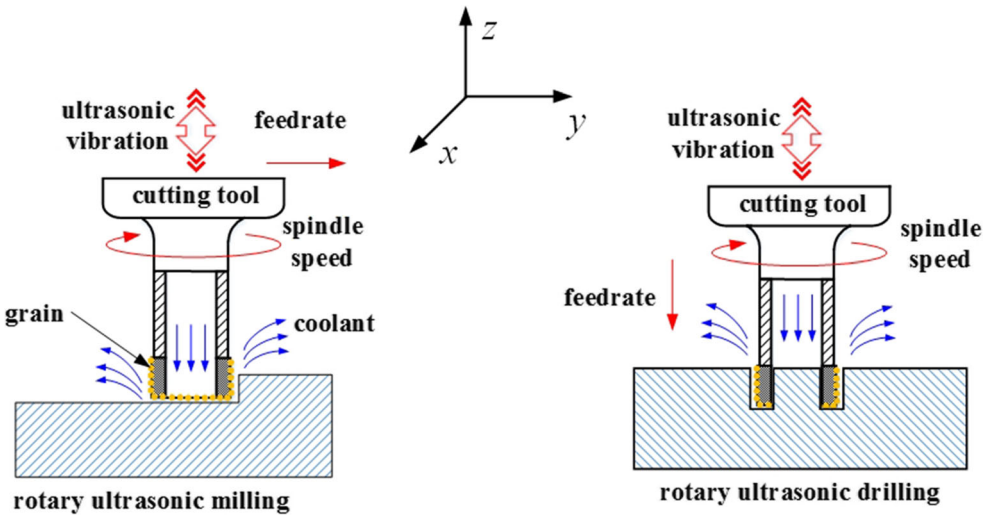

Fig. 1 Schematic of the RUM process

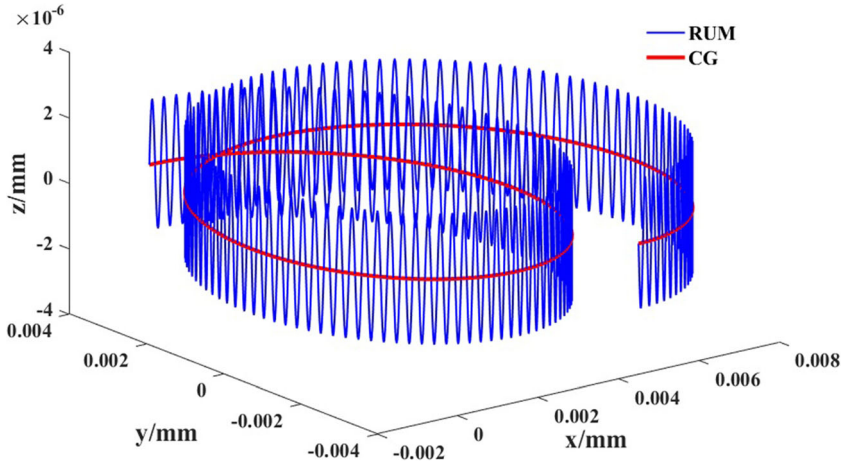

Fig. 2 Trajectories of an abrasive grain in RUM and CG

ceramics both in UVAS tests and CS tests. However, the critical cutting depth increased by 56.25% in UVAS. Zhang et al. [25, 26] investigated the anisotropy in the material removal characteristics for the three directions of the KDP crystal by UVAS tests and CS tests. Feng et al. [27] used the same methods to study the scratching characteristics of high-volume fraction SiCp/Al composites. The results in UVAS revealed that compared with those of CS, the scratching force and the removal rate were smaller and higher, respectively. However, the micromaterial removal process and the influence of ultrasonic vibration on the material were not analyzed. The material removal mechanism in RUM of SiCp/Al composites has not been explored clearly yet.

The material removal mechanism in RUM of SiCp/Al composites is investigated in this work and the influence of ultrasonic vibration on the machining process is explained through theoretical analysis and experiments. In this study, both UVAS tests and CS tests were performed on a rotary ultrasonic machine using an in-house-developed conical diamond tool. The influence of ultrasonic vibration on the machining process was analyzed. The experimental setup and the experimental results were presented in detail. Furthermore, the material removal mechanism in RUM of SiCp/Al composites was explicated by comparing the material removal characteristics in UVAS tests and CS tests.

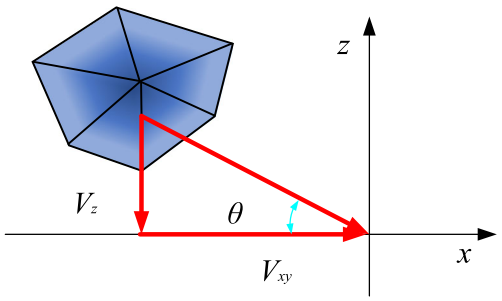

Fig. 3 Definition of penetration angle

2 Influence of ultrasonic vibration on the machining process

RUM combines conventional ultrasonic vibrating machining and grinding technology. Owing to the ultrasonic vibration, the kinematic characteristics of the cutting tool and the properties of the material have changed and differ from those in CG process.

2.1 Influence on the cutting tool

The motional trajectory of an abrasive grain on the cutting tool is described by the following equation:

$$\gamma(t)=\begin{pmatrix}x(t)\\y(t)\\z(t)\end{pmatrix}=\begin{pmatrix}r\cdot\sin\left(\frac{2\pi n}{60}t\right)+\int v_x(t)\mathrm{d}t+x_0\\r\cdot\cos\left(\frac{2\pi n}{60}t\right)+\int v_y(t)\mathrm{d}t+y_0\\A\cdot\sin(2\pi\mathrm{ft})+\int v_z(t)\mathrm{d}t+z_0\end{pmatrix} \quad (1)$$

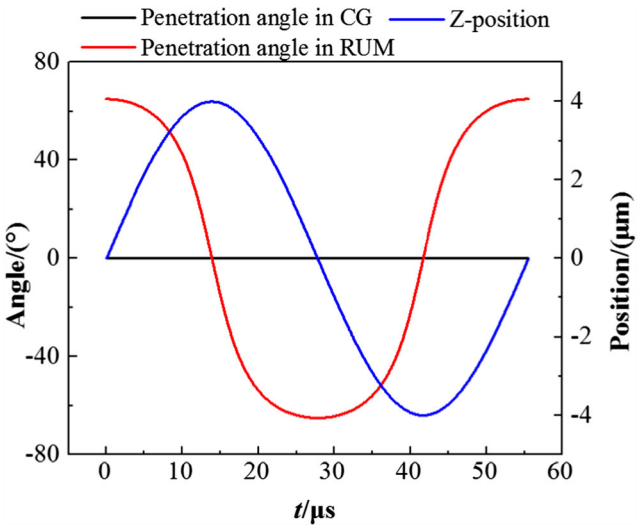

Fig. 4 Penetration angle during one vibration cycle

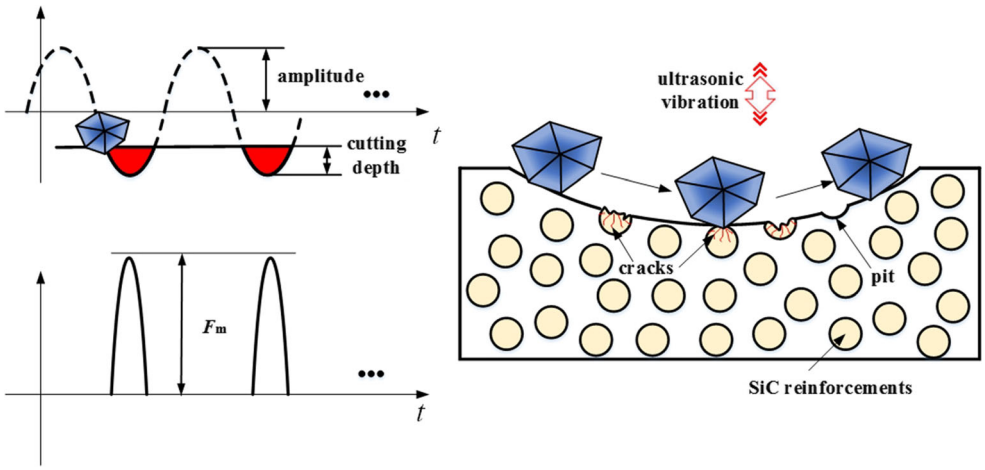

Fig. 5 Influence of ultrasonic vibration on machining process

where v_x, v_y, v_z represent the components of the feed velocity; x_0, y_0, z_0 represent the components of the initial position; r is the distance from the abrasive grain to the center of the cutting tool; n is the spindle speed; A is the ultrasonic amplitude and f is the frequency of ultrasonic vibration. Figure 2 shows the trajectory of an abrasive grain in RUM and CG when the machining of faces is considered. As the figure shows, the abrasive grain moves only on the x-y-plane in CG but travels in a three-dimensional space in RUM. The machining process becomes discontinuous and the cutting length increases.

Calculation of the time derivative $\frac{d}{dt}\gamma(t)$ yields the following relation for the velocity of the grain:

$$\gamma'(t) = \begin{pmatrix} V_x(t) \\ V_y(t) \\ V_z(t) \end{pmatrix} = \begin{pmatrix} \frac{2\pi n}{60} \cdot r \cdot \cos\left(\frac{2\pi n}{60} t\right) + v_x(t) \\ -\frac{2\pi n}{60} \cdot r \cdot \sin\left(\frac{2\pi n}{60} t\right) + v_y(t) \\ 2\pi f A \cdot \cos(2\pi f t) + v_z(t) \end{pmatrix} \tag{2}$$

The rotational movement is superposed with the vertical vibration, thereby preventing perpendicular indentation of the abrasive grain into the workpiece. The penetration angle θ, as shows in Fig. 3, which is dependent on the angular position of the abrasive grain can be calculated from:

$$\theta(t) = \tan^{-1}\left(\frac{V_z}{V_{xy}}\right) = \tan^{-1}\left(\frac{2\pi f A \cdot \cos(2\pi f t) + v_z}{\sqrt{\left(\frac{2\pi n}{60} \cdot r \cdot \cos\left(\frac{2\pi n}{60} t\right) + v_x\right)^2 + \left(-\frac{2\pi n}{60} \cdot r \cdot \sin\left(\frac{2\pi n}{60} t\right) + v_y\right)^2}}\right) \tag{3}$$

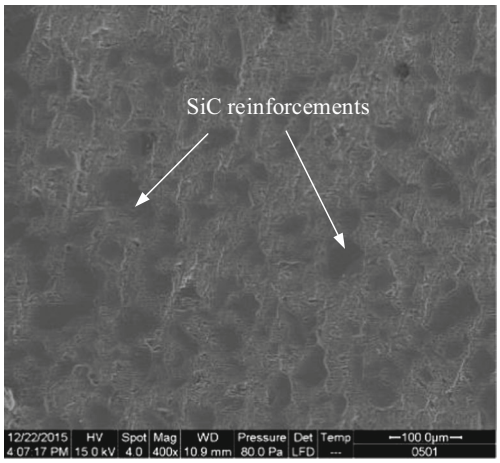

Fig. 6 Polished surface of the workpiece

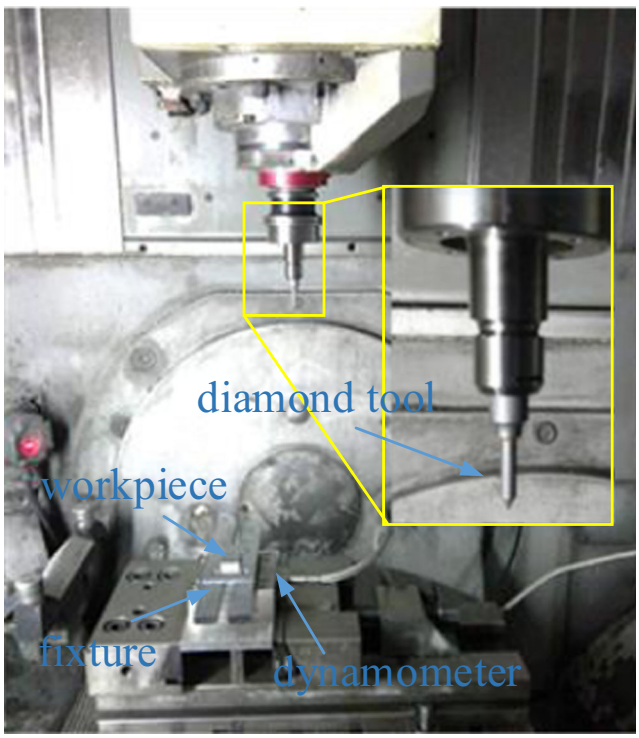

Fig. 7 Experimental setup

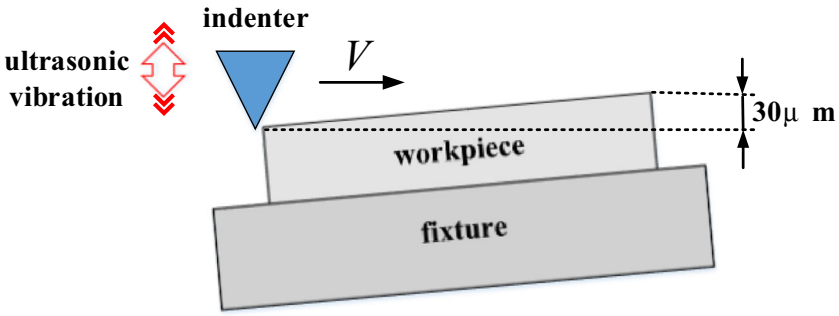

Fig. 8 Schematic of experimental procedure

Therefore, $\theta = 0^{\circ}$ and $\theta = 90^{\circ}$ indicate parallel and perpendicular movement to the *x*-*y*-plane, respectively.

Figure 4 shows the variation of the penetration angle θ and the *z*-position of the abrasive grain in one vibration cycle. The maximum angle θ_{max} occurs at a *z*-position of zero. However, at the maximum value of the *z*-position, the velocity in the *z* direction equals zero and hence, the angle is also zero. This leads to a non-static penetration angle and in turn, a constantly changing material indentation angle and material exit angle during one rotation cycle.

2.2 Influence on the material

The ultrasonic vibration changes the kinematic characteristics of the abrasive grain and also has a certain effect on the material. In RUM, the impact time of the abrasive grain is very short and the high frequency of the ultrasonic vibration results in a high strain rate of material. According to [28], the flow stress and the strain-rate hardening effect of the Al matrix increases with increasing strain rates. The Al matrix is enhanced by the ultrasonic vibration.

In addition, the acceleration along the *Z* direction $a_z(t)$ can be determined by from the time derivation $\frac{d}{dt}\gamma'(t)$ and is given:

$$a_z(t) = -4\pi^2 f^2 A \cdot \sin(2\pi \mathrm{ft}) + \frac{d}{dt} v_z(t) \tag{4}$$

Hence, for *f* and *A* of 20 kHz and 5 μm, respectively, a maximum instantaneous acceleration of $7.9 \times 10^4 m/s^2$ is realized for the abrasive grain. The inertial force $F(t)$ can be calculated from (v_z is zero in face machining):

$$F(t) = \mathrm{ma}_z(t) = -4m\pi^2 f^2 A \cdot \sin(2\pi \mathrm{ft}) \tag{5}$$

where *m* is the weight of the abrasive grain. The inertia force has an important influence on the interaction between the abrasive grain and the workpiece. In fact, the force on the abrasive grain can yield cracks in SiC reinforcements so that they can be removed more easily. Figure 5 illustrates the influence of ultrasonic vibration on the machining process. These analyses would be verified by experiments in the next section.

3 Experimental setup

3.1 Material and equipment

SiCp/Al composites whose volume fraction is 56% were considered in the experiments. Prior to the experiments, the top surface of the 30 mm × 20 mm × 5 mm workpiece was carefully polished and examined by scanning electron microscope (SEM), as seen in Fig. 6. An in-house-developed diamond indenter was used as the scratching tool in the experiments. A conical diamond was brazed on a special shank that can be fixed to the ultrasonic spindle to obtain ultrasonic vibration. The vertical angle and the nose radius of the diamond indenter are 60° and 100 μm, respectively.

The experiments were performed on a rotary ultrasonic machine (Ultrasonic 50, DMG, Germany) composed of an ultrasonic spindle, a feed system, and a coolant supply system

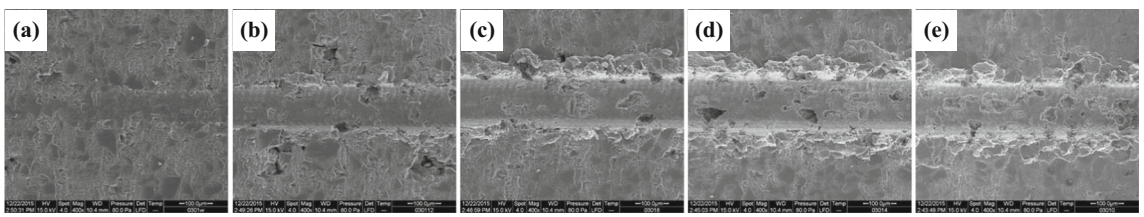

Fig. 9 SEM images in (a) the beginning; (b), (c), (d) the middle; (e) the end of the groove in the UVAS

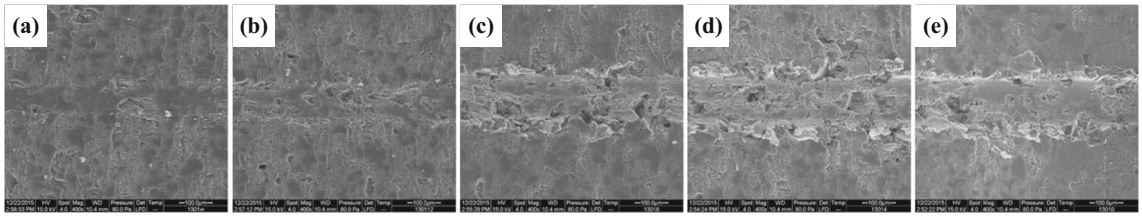

Fig. 10 SEM images in (a) the beginning; (b), (c), (d) the middle; (e) the end of the groove in the CS

(typical coolant: Grindex 10 CO, Blaser). The maximum ultrasonic power and the frequency range of ultrasonic vibration for this machine are 300 W and 16.5~30 kHz, respectively. As Fig. 7 shows, the diamond indenter was installed in the ultrasonic spindle through an ER16 cone fitting. When ultrasonic vibration function is turned on, the ultrasonic amplitude of the indenter is 5 μm measured by a laser fiber vibrometer. The experiments turn to be CS tests when this function is turned off. The surface-processed SiCp/Al composites workpiece was fixed on a fixture using AB glue and the fixture was screwed on the dynamometer (9256C2, Kistler Instrument Corp., Switzerland). This dynamometer was used to record the scratching forces during the experiments.

3.2 Experimental procedure

As Fig. 8 shows, under non-cooling conditions, the diamond indenter moved from the left side to the 30 μm higher right side of the workpiece with a certain velocity. The experimental parameters were as follows: the scratching depth was 0~30 μm, the moving velocity was 24,000 mm/min, the frequency of ultrasonic vibration was 18,850 Hz, and the scratching length was 20 mm. Both UVAS and CS tests were conducted on the same workpiece with a separation of 2 mm.

After the scratch tests, the workpiece was ultrasonically cleaned for 10 min in anhydrous alcohol. The morphology of each cleaned scratching groove was observed via SEM.

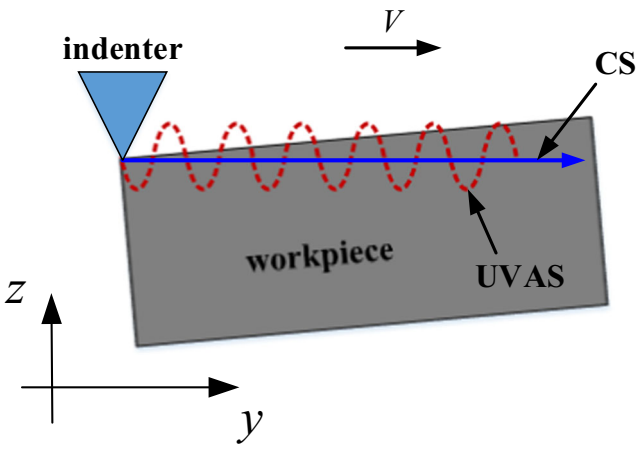

Fig. 11 Schematic of indenter trajectories in UVAS and CS

4 Results and discussion

4.1 The morphologies of scratching grooves

Differences in the material removal characteristics between UVAS and CS are revealed via SEM of the workpiece after scratching with and without ultrasonic vibration. The SEM images in Figs. 9 and 10 show the different regions of the groove formed in the UVAS and CS tests, respectively. Figure 9(a) and Fig. 10(a) are at the beginning of grooves; Figure 9(b, c, d) and Fig. 10(b, c, d) are at the middle of grooves; Figure 9(e) and Fig. 10(e) are at the end of grooves.

The scratching process in both UVAS and CS grooves consists of three stages: (1) plastic deformation period. As shown in Fig. 9(a) and Fig. 10(a), the surface of each groove was very smooth and there was no material removal. The grooves showed a stage of plastic deformation; (2) plowing period. As Fig. 9(b) and Fig. 10(b) show, when the scratching depth increased, the deformed materials were forced to flow toward both sides of the groove, thereby forming a pile-up. No material removal occurred here; (3) cutting period. Chips were formed when the scratching depth increased. They can be seen in Fig. 9(c, d, e) and Fig. 10(c, d, e). The scratching depth plays a key role in determining the stages during the scratching process. However, the scratching morphologies of SiCp/Al composites differ from those of monolithic metal that can form continuous chips, and also not like scratching tests of monolithic ceramic, where lots of cracks form on the surface. Scratching tests of SiCp/Al composites form discontinuous chips and it has not cracks but different kinds of holes. Cracks can only be observed in SiC reinforcements.

The material removal characteristics of the UVAS significantly differ from the characteristics of the CS. In the groove of UVAS, the surface of the Al matrix was considerably smoother than the groove in CS. Moreover, the SiC reinforcements were broken into small particles and then completely removed, leaving lots of holes on the surface of the workpiece. However, in the groove of CS, the surface of the Al matrix was very coarse and the SiC reinforcements were broken into large pieces which undergo significant fracture.

According to the kinematic analysis of diamond grain, their kinematic characteristics in UVAS and CS are different with each other. Figure 11 illustrates trajectories of the indenter in UVAS and CS. The indenter in UVAS moves along the *y*-axis

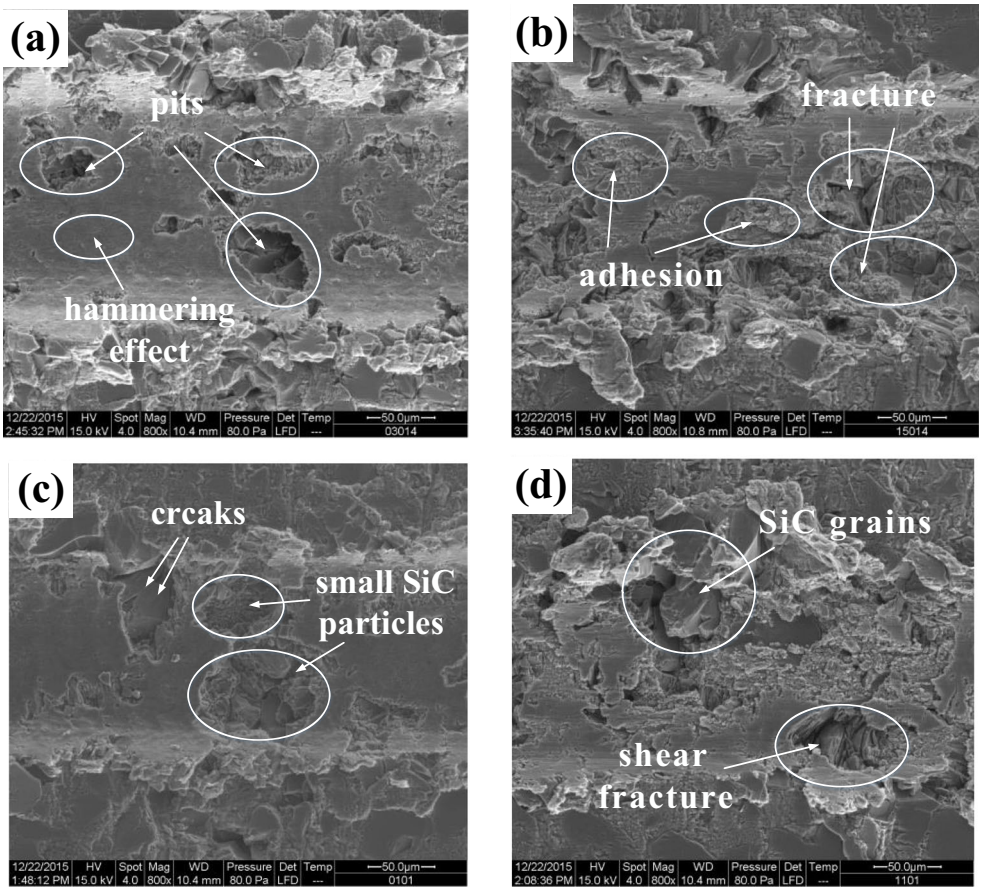

Fig. 12 The material removal mechanism. **a** Impact and hammering effect in the UVAS. **b** Adhesion in the CS. **c** Cracks in SiC reinforcements during the UVAS. **d** Shear fracture in SiC reinforcements during the CS

at a constant velocity and simultaneously vibrates along the *z*-axis with a high frequency. The velocity of the indenter is parallel to the *y*-axis and the scratching depth increases gradually leading to plastic deformation, plowing, and cutting. The ultrasonic vibratory velocity is vertically downward to the workpiece, thereby resulting in the hammering on the surface. During the CS process, the velocity of the indenter is parallel to the *y*-axis only.

Because of the different kinematic characteristics in UVAS and CS, the material removal mechanism becomes different. As shown in Fig. 12a, the Al matrix endured continuous ultrasonic impact and the surface was constantly squeezed. The material underwent plastic deformation and the surface became very smooth and there was no adhesion. In contrast, the SiC reinforcements are brittle and barely undergo plastic deformation. So they broke into small particles and were easily removed under ultrasonic vibration of the indenter. These phenomena can also be seen in Fig. 12c. The impact force which ultrasonic vibration brought produced many cracks in SiC reinforcements.

As Fig. 12b shows, the indenter contacted with the material all the time during the scratching process and the Al matrix was adhered away forming a very coarse surface. Shear fracture occurred in SiC reinforcements. These phenomena can also be seen in Fig. 12d. SiC reinforcements cannot break into small particles.

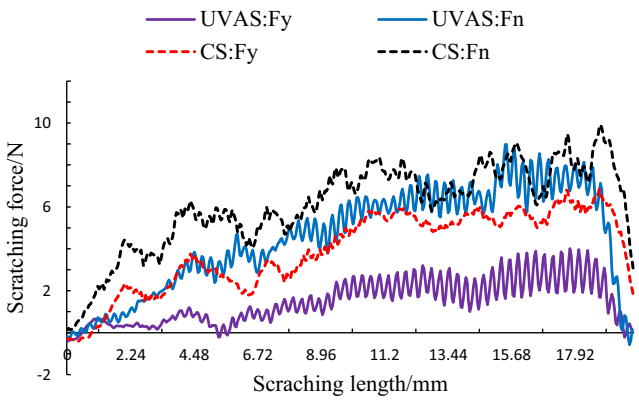

Fig. 13 Comparison of the scratching force between UVAS and CS

4.2 Scratching force and coefficient of friction

The characteristics of the scratching force reflect the scratching process during the experiments. In the tests, the axial force (F_n) and the tangential force (F_y) were considerably larger than the normal force in tests; hence, we only focused on F_n and F_y. The results revealed that F_n and F_y increase gradually with increasing scratching depth during the scratching process in UVAS and CS which can be seen

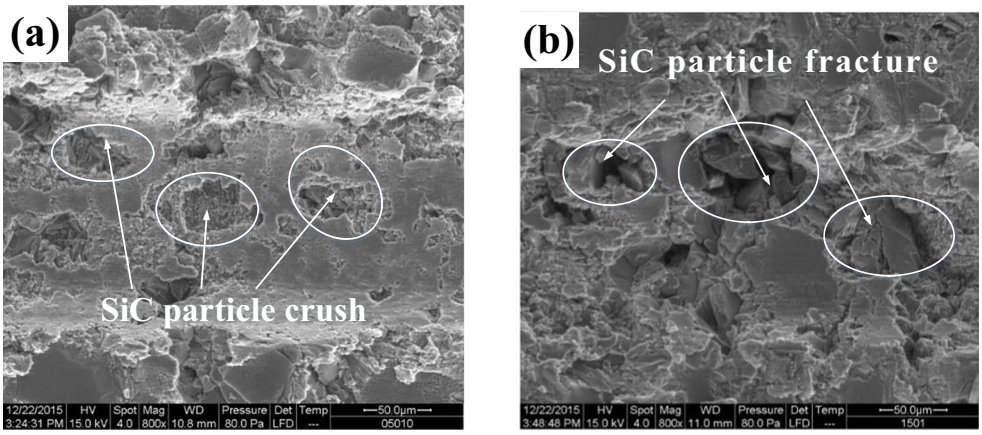

Fig. 14 Comparison of the scratching morphology **a** in UVAS and **b** in CS

in Fig. 13. However, the scratching forces in CS fluctuated sharply during increasing process, whereas those in UVAS increased continuously in the entire process and there are sinusoidal waves at local areas because of ultrasonic vibration. The values of the scratching forces in CS were also larger than those in UVAS in general.

SiCp/Al composites are inhomogeneous materials. When the indenter scratches the Al matrix, the scratching force is small. However, when the indenter scratches the SiC reinforcements, the scratching force will increase abruptly and decrease after SiC reinforcements fracture. Figure 14a, b showed the comparison of the scratching morphology in UVAS and CS, respectively. In Fig. 14a, because of the hammering effect of ultrasonic vibration, SiC reinforcements broke into small particles and they were more easily removed in UVAS. Therefore, the scratching force in UVAS was more stable and smaller than that in CS.

The COF is defined as the ratio of the tangential force and the axial force (i.e., COF = F_y/F_n). In Fig. 15, the COF both in UVAS and CS increased slightly with the increase of the scratching depth. The COF in UVAS was smaller than it in CS while the COF in CS was more stable than it in UVAS. In CS, adhesion played a significant role in the Al matrix leading to an increase in tangential force. Moreover, owing to ultrasonic vibration, the scratching depth of the indenter changed constantly. The tangential force and the axial force were characterized by a periodic sinusoidal change in UVAS. As a result, the COF in CS became larger and more stable than it in UVAS. The friction between the indenter and the workpiece in CS was more violent than that in UVAS.

4.3 Material removal process of SiCp/Al composites

Different interactions between the indenter and the workpiece occurred during the process of scratching SiCp/Al composites. Figure 16a, b revealed there are three situations in the grooves, where the (1) indenter scratched only on the Al matrix. The Al matrix could easily be removed relatively. The finished surface in UVAS was very smooth for hammering effect, whereas the finished surface in CS was very coarse; (2) the indenter scratched only on the SiC reinforcements. They broke into small particles and were removed completely in UVAS, while they occurred in shear fracture in CS; (3) the indenter scratched into the SiC reinforcements from the Al matrix, or the indenter scratched into the Al matrix from the SiC reinforcements. Because SiC reinforcements are much harder than aluminum, when the indenter scratched into SiC reinforcements, the scratch force increases sharply and the SiC reinforcements experienced a severe shock. In contrast, when the indenter scratched out of the SiC reinforcements, the indenter transited to scratch the Al matrix very gently. Hence,

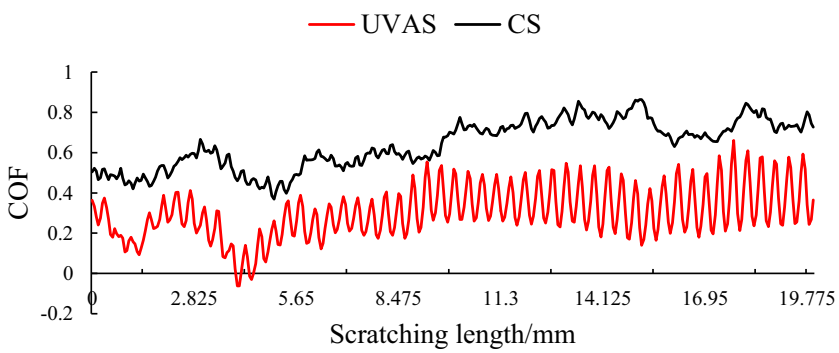

Fig. 15 Comparison of the COF between UVAS and CS

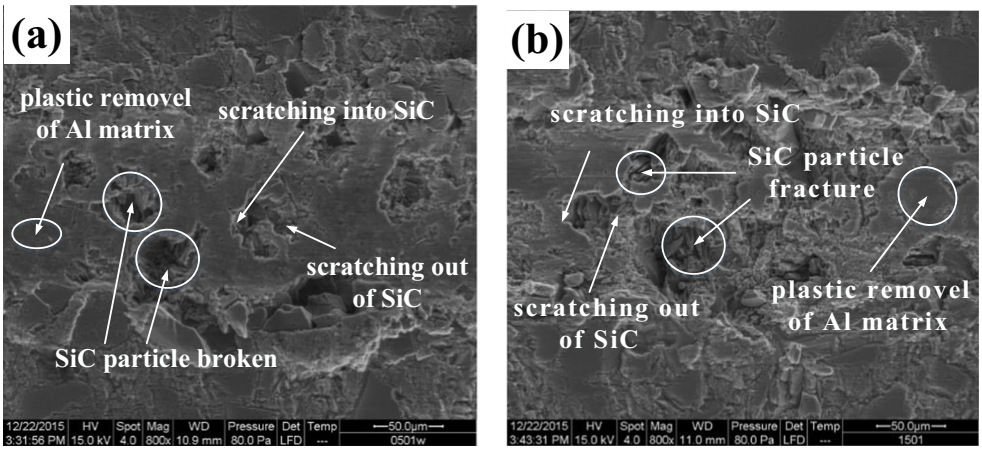

Fig. 16 Different interactive situations during the scratching process **a** in UVAS and **b** in CS

the bottom surface of the hole was typically inclined. These phenomena can also be seen in Fig. 16.

During the scratching process, when the cutting depth is small, the Al matrix underwent plastic deformation, whereas SiC reinforcements endured elastic deformation or are pressed into the Al matrix. When the cutting depth increased, the Al matrix suffered severe deformation in a short time. Due to the presence of SiC reinforcements, the composites cannot form continuous chips. The Al matrix and the SiC reinforcements affected with each other. They endured a deformation compatibility.

Figure 17a, b is two-dimensional morphology and three-dimensional morphology of the rotary ultrasonic machined surface, respectively. The removal characteristics of the Al matrix and the SiC reinforcements are different. The surface of the Al matrix was continuous and smooth and enhanced by the ultrasonic vibration. However, SiC reinforcements were broken down and formed many pits on the surface. It can be seen that most of the defects in the machined surface occurred in the SiC reinforcements. So the removal mode of SiC reinforcements played an important role in the formation of the machined surface. Appropriate processing parameters should be selected to improve the removal efficiency of SiC reinforcements and the final machining quality of SiCp/Al composites.

5 Conclusions

Differences in the material properties of the Al matrix and the SiC reinforcement lead to the special machining characteristics of SiCp/Al composites. The material removal mechanism in RUM of high-volume fraction SiCp/Al composites was investigated via UVAS tests and CS tests. In addition, the influence of ultrasonic vibration on the machining process was analyzed. The morphology of the scratching surfaces and the scratching forces were investigated and the material removal process was described in detail. The conclusions can be summarized as follows:

1) Ultrasonic vibration changes the kinematic characteristics of the cutting tool and the properties of the SiCp/Al composites. The abrasive grain moves in a three-dimensional space in RUM and its machining process becomes discontinuous. The Al matrix is enhanced by the ultrasonic vibration and the SiC reinforcements can be removed more easily because of many micro cracks.
2) The scratching forces and the COF of ultrasonic scratching in UVAS tests are smaller than those in CS tests. The friction between the grain and the workpiece is reduced and the adhesion of aluminum matrix is weakened in UVAS tests.

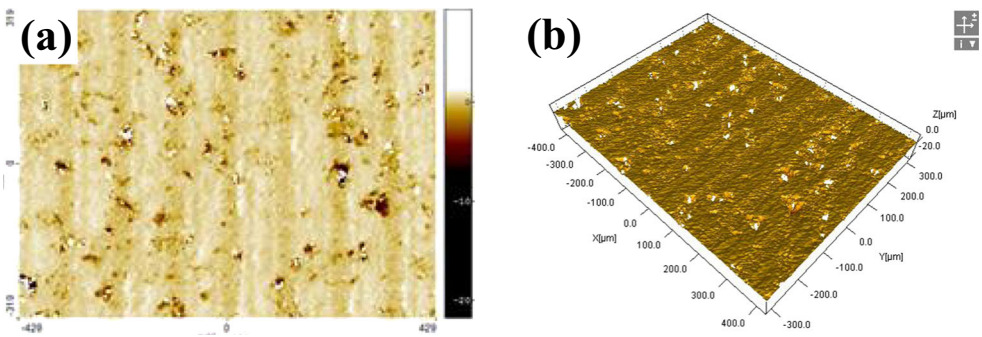

Fig. 17 Morphologies of the rotary ultrasonic machined surface **a** two-dimensional morphology and **b** three-dimensional morphology

3) Abrasive grain scratching of the SiCp/Al composites consists of three situations. On the changing phases of two component materials, the cutting force increases sharply and the SiC reinforcements experience a sudden impact and endure serious particle breakage.
4) The removal mode of SiC reinforcements plays a decisive role in the formation of the machined surface. If appropriate ultrasonic machining parameters are selected, SiC reinforcements can be removed more smoothly, and the surface quality of SiCp/Al composites can be effectively improved.

Funding information This research received financial support from the National Natural Science Foundation of China (Grant No. 51475260 and No. 5171101622) and the Beijing Natural Science Foundation (Grant No. 3141001).

References

1. Ren S, Qu X, Guo J, He X, Qin M, Shen X (2009) Net-shape forming and properties of high volume fraction SiCp/Al composites. J Alloy Compd 484:256–262. https://doi.org/10.1016/j.jallcom.2009.04.074
2. Xiu Z, Yang W, Dong R, Hussain M, Jiang L, Liu Y, Wu G (2015) Microstructure and mechanical properties of 45 vol.% SiCp/7075Al composite. J Mater Sci Technol 31:930–934. https://doi.org/10.1016/j.jmst.2015.01.012
3. Sahin Y, Acılar M (2003) Production and properties of SiCp-reinforced aluminium alloy composites. Compos Part A: Appl Sci Manufac 34:709–718. https://doi.org/10.1016/S1359-835X(03)00142-8
4. Kevorkijan VM (1999) Aluminum composites for automotive applications: a global perspective. Jom-Us 51:54–58. https://doi.org/10.1007/s11837-999-0224-2
5. Lee HS, Jeon KY, Kim HY, Hong SH (2000) Fabrication process and thermal properties of SiCp/Al metal matrix composites for electronic packaging applications. J Mater Sci 35(24):6231–6236. https://doi.org/10.1023/A:1026749831726
6. Cui Y, Wang L, Ren J (2008) Multi-functional SiC/Al composites for aerospace applications. Chin J Aeronaut 21(6):578–584. https://doi.org/10.1016/S1000-9361(08)60177-6
7. Tosun G, Muratoglu M (2004) The drilling of Al/SiCp metal–matrix composites. Part II: workpiece surface integrity. Compos Sci Technol 64:1413–1418. https://doi.org/10.1016/j.compscitech.2003.07.007
8. Tosun G, Muratoglu M (2004) The drilling of an Al/SiCp metal-matrix composites. Part I: microstructure. Compos Sci Technol 64:299–308. https://doi.org/10.1016/S0266-3538(03)00290-2
9. Dandekar CR, Shin YC (2009) Multi-step 3-D finite element modeling of subsurface damage in machining particulate reinforced metal matrix composites. Compos Part A: Appl Sci Manufac 40:1231–1239. https://doi.org/10.1016/j.compositesa.2009.05.017
10. Zhou L, Hou N, Huang S, Xu L (2014) An experimental study on formation mechanisms of edge defects in orthogonal cutting of SiCp/Al composites. Int J Adv Manuf Technol 72:1407–1414. https://doi.org/10.1007/s00170-014-5743-5
11. Li X, Seah WKH (2001) Tool wear acceleration in relation to workpiece reinforcement percentage in cutting of metal matrix composites. Wear 247:161–171. https://doi.org/10.1016/S0043-1648(00)00524-X
12. Ciftci I, Turker M, Seker U (2004) Evaluation of tool wear when machining SiCp-reinforced Al-2014 alloy matrix composites. Mater Des 25:251–255. https://doi.org/10.1016/j.matdes.2003.09.019
13. Singh RP, Singhal S (2004) Rotary ultrasonic machining: a review. Adv Manuf Processes 31(14):1795–1824. https://doi.org/10.1080/10426914.2016.1140188
14. Gong H, Fang FZ, Hu XT (2010) Kinematic view of tool life in rotary ultrasonic side milling of hard and brittle materials. Int J Mach Tool Manu 50:303–307. https://doi.org/10.1016/j.ijmachtools.2009.12.006
15. Zhang C, Zhang J, Feng P (2013) Mathematical model for cutting force in rotary ultrasonic face milling of brittle materials. Int J Adv Manuf Technol 69:161–170. https://doi.org/10.1007/s00170-013-5004-z
16. Debnath K, Singh I, Dvivedi A (2015) Rotary mode ultrasonic drilling of glass fiber-reinforced epoxy laminates. J Compos Mater 49:949–963. https://doi.org/10.1177/0021998314527857
17. Kadivar MA, Akbari J, Yousefi R, Rahi A, Nick MG (2014) Investigating the effects of vibration method on ultrasonic-assisted drilling of Al/SiCp metal matrix composites. Robot Cim-Int Manuf 30:344–350. https://doi.org/10.1016/j.rcim.2013.10.001
18. Zhang C, Feng P, Wu Z, Yu D (2011) Mathematical modeling and experimental research for cutting force in rotary ultrasonic drilling. J Mech Eng 47(15):149–155. https://doi.org/10.3901/JME.2011.15.149
19. Ahmed Y, Cong WL, Stanco MR, Xu Z, Pei Z, Treadwell C, Zhu Y, Li Z (2012) Rotary ultrasonic machining of alumina dental ceramics: a preliminary experimental study on surface and subsurface damages. J Manuf Sci Eng 134(6):67–75. https://doi.org/10.1115/1.4007711
20. Lv D, Huang Y, Tang Y, Wang H (2013) Relationship between subsurface damage and surface roughness of glass BK7 in rotary ultrasonic machining and conventional grinding processes. Int J Adv Manuf Technol 67:613–622. https://doi.org/10.1007/s00170-012-4509-1
21. Huang S, Yu X, Wang F, Xu L (2015) A study on chip shape and chip-forming mechanism in grinding of high volume fraction SiC particle reinforced Al-matrix composites. Int J Adv Manuf Technol 80:1927–1932. https://doi.org/10.1007/s00170-015-7138-7
22. Zhou L, Huang S, Xu L, Bai D, Zhao P (2013) Drilling characteristics of SiCp/Al composites with electroplated diamond drills. Int J Adv Manuf Technol 69:1165–1173. https://doi.org/10.1007/s00170-013-5096-5
23. Zhang C, Feng P, Zhang J (2013) Ultrasonic vibration-assisted scratch-induced characteristics of C-plane sapphire with a spherical indenter. Int J Mach Tool Manu 64:38–48. https://doi.org/10.1016/j.ijmachtools.2012.07.009
24. Cao J, Wu Y, Lu D, Fujimoto M, Nomura M (2014) Material removal behavior in ultrasonic-assisted scratching of SiC ceramics with a single diamond tool. Int J Mach Tool Manu 79:49–61. https://doi.org/10.1016/j.ijmachtools.2014.02.002
25. Zhang J, Wang D, Feng P, Wu Z, Zhang C (2016) Material removal characteristics of KDP crystal in ultrasonic vibration-assisted scratch process. Mater Manuf Process 31(8):1037–1045. https://doi.org/10.1080/10426914.2015.1070423

26. Zhang J, Wang D, Feng P, Wu Z, Yu D (2015) Effect of processing parameters of rotary ultrasonic machining on surface integrity of potassium dihydrogen phosphate crystals. Adv in Mech Eng 7(9): 1–10. https://doi.org/10.1177/1687814015606329
27. Feng P, Liang G, Zhang J (2014) Ultrasonic vibration-assisted scratch characteristics of silicon carbide-reinforced aluminum matrix composites. Ceram Int 40:10817–10823. https://doi.org/10.1016/j.ceramint.2014.03.073
28. Tan ZH, Pang BJ, Qin DT, Shi JY, Gai BZ (2008) The compressive properties of 2024Al matrix composites reinforced with high content SiC particles at various strain rates. Mater Sci Eng A 489:302–309. https://doi.org/10.1016/j.msea.2007.12.021